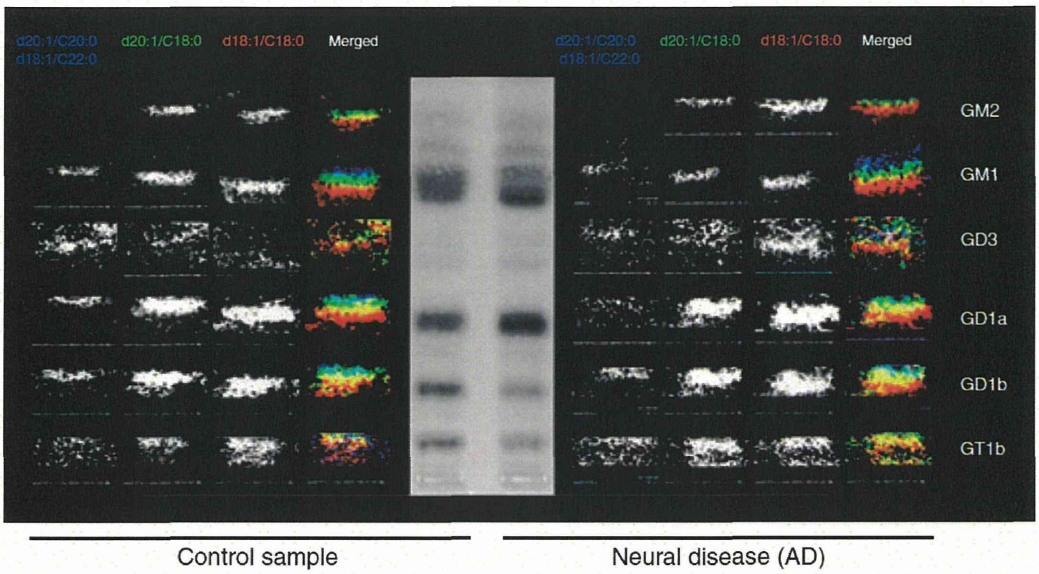

Fig. 1. TLC-Blot-MALDI-QIT-TOF-MS Imaging of Hippocampus Gray Matter Gangliosides

The raster scan of the polyvinylidene difluoride membrane was performed automatically. The number of laser irradiations was 5 shots in each spot. The interval of data points was 200 lm. The color red indicates a d18:1 sphingosine-containing signal, the color green a d20:1 sphingosine-containing signal, and the color blue a d18:1/C22:0- or d20:1/C20:0-containing signal. Merged images of these are shown on the right side of each panel. (Reprinted from ref. 60 with permission from Blackwell Publishing.)

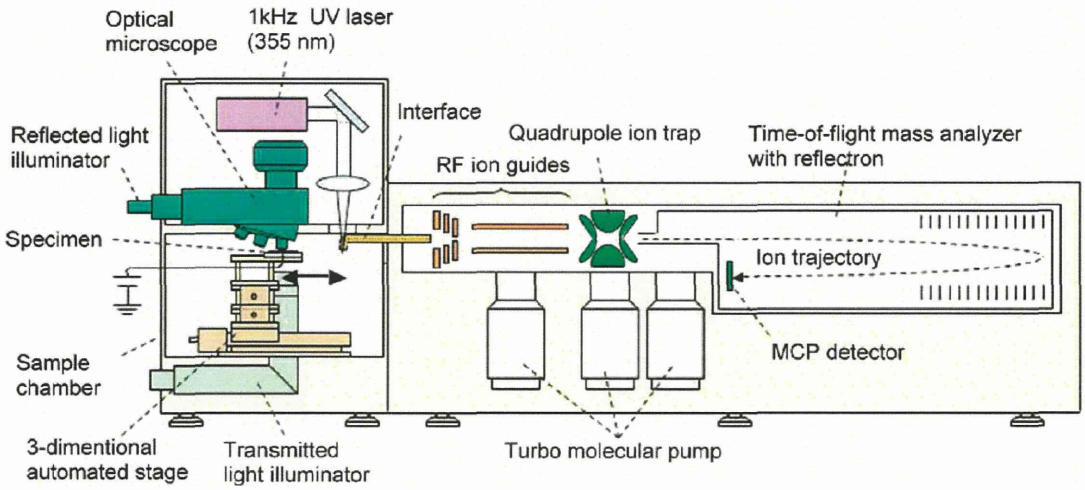

Fig. 2. Schematic Diagram Showing the Mass Microscope

(Reprinted from ref. 66 with permission from the American Chemical Society.)

recent years, MALDI imaging has resulted in many developments for assessing the localization of molecular species in biological samples. Several applications represent the direct entailment of this technology to basic clinical research. Here, we discuss the recent developments concerning MALDI-IMS.

2. TARGETS OF ANALYSIS BY MALDI-IMS

2.1. Imaging of Glycosphingolipids Glycosphingolipids (GSLs) play important roles in various brain functions. To investigate the mechanisms of brain function in more detail, it is necessary to understand the composition and function of GSLs. We have studied GSLs in previous research.[6,14,54,55] Thin-layer chromatography (TLC) is routinely used for the separation and partial characterization of neutral and acidic GSLs and phospholipids in mixtures.[56–58] However, even under optimized TLC conditions, TLC characterization of individual GSLs does not yield unambiguous structural information. Information regarding the compositions of these highly complex mixtures remains limited. The same sugar moiety in different GSLs may migrate to different positions owing to differences in their ceramide structures. Multi-stage MS (MS^n) analysis can supply information on each ceramide structure. However, it is difficult to identify individual molecular species by MS alone. Therefore, by combining TLC and MS, we were able to obtain a complete set of information on GSLs.

Our group has used MALDI-MS/MS to study colon cancer liver metastasis in 3 μm thick tissue sections. MS/MS investigations of normal and cancerous cells revealed

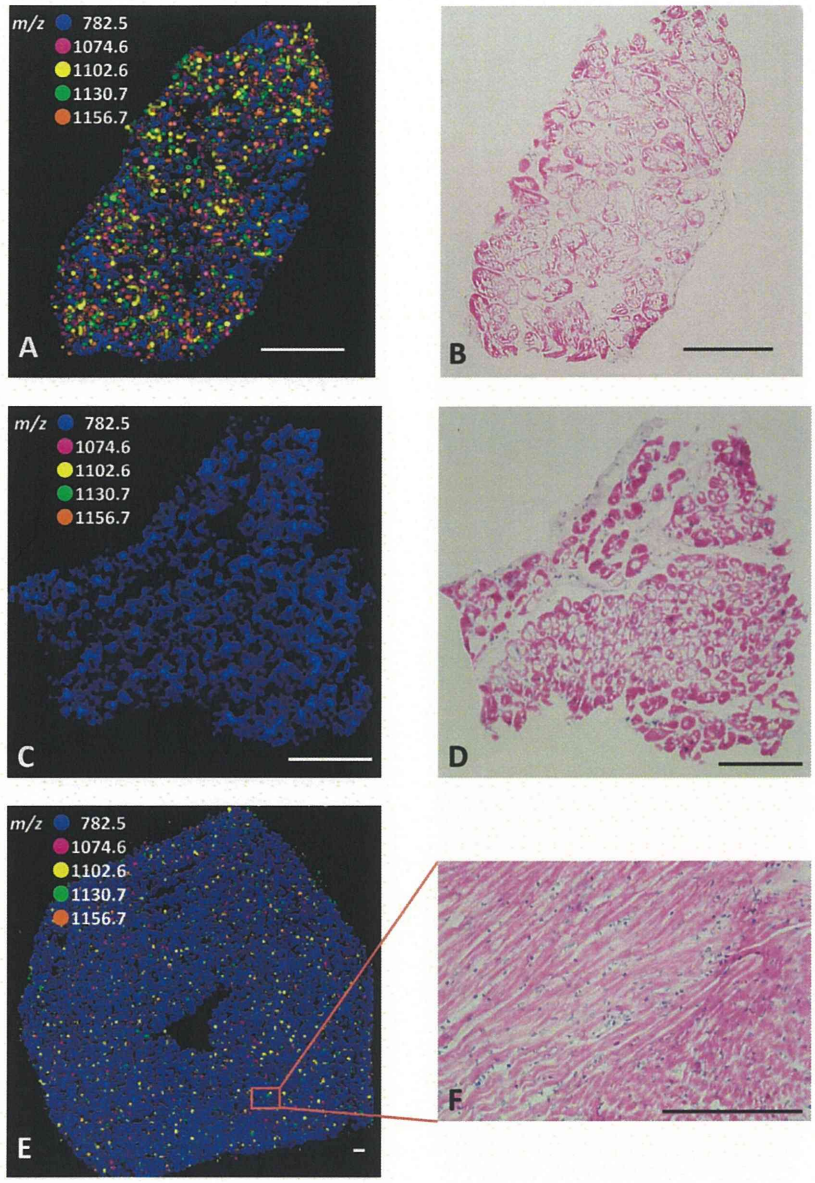

Fig. 3. IMS and Histology of the Samples

We constructed a figure by plotting the positions of the *m/z* 782.5, 1074.6, 1102.6, 1130.7 and 1156.7 peaks. When we compared (A) IMS with (B) a hematoxylin and eosin-stained section, the peaks of Gb3s were more densely packed in cardiomyocytes with vacuolar degeneration, and the Gb3s existed together in some parts and separately in others. (C,D) In contrast, Gb3 was not detected in a control sample from a patient with secondary myocardial degenerative changes with aortic regurgitation. (E,F) Gb3s were also detected on IMS in the heart of a mouse with Fabry's disease even though there was no evidence of vacuolar changes in the myocardium on light microscopy. Bar, 200 μm. (Reprinted from ref. 67 from Official Journal of the Japanese Circulation Society.)

that the cancerous cells accumulated sphingomyelin.[47] We have also studied the localization of seminolipids in mouse testis during testicular maturation, and the organ-specific distribution of lysophosphotidylcholine and triacylglycerol in mouse embryos using IMS.[45,59] Recently, our group has developed a TLC-Blot-MALDI-TOF-IMS system which can separate and partially characterize acidic and neutral GSLs. Here, we describe gangliosides identified from a control patient and a patient with Alzheimer's disease using TLC-Blot-MALDI-TOF-MS imaging of the hippocampus gray matter (Fig. 1). In the Alzheimer's patient, the GM2 and GD3 ganglioside bands appeared to be clearer than those of the control. The relative increases in d18:1 sphingosine-containing gangliosides in the patient with Alzheimer's disease are also expressed in this image.[60]

2.2. Imaging of Proteins and Peptides Immunohistochemistry has been commonly used for profiling protein distribution in tissue sections. In this approach, antibodies are needed to detect specific proteins. Other genomic and proteomic approaches cannot be applied to biopsies as the quantity of sample available is only very small.[14,61–63] Our group has analyzed *SCRAPPER* (A protein we first reported that is localized in neuronal synapses.)[6] knockout mouse by utilizing a proteomic approach based on an IMS technique.[64] We have also demonstrated that the denaturation process and detergent-supplemented trypsin solution can improve the protein digestion efficiency for direct tissue analysis with IMS.[65] We recently developed a formalin-fixed paraffin-embedded

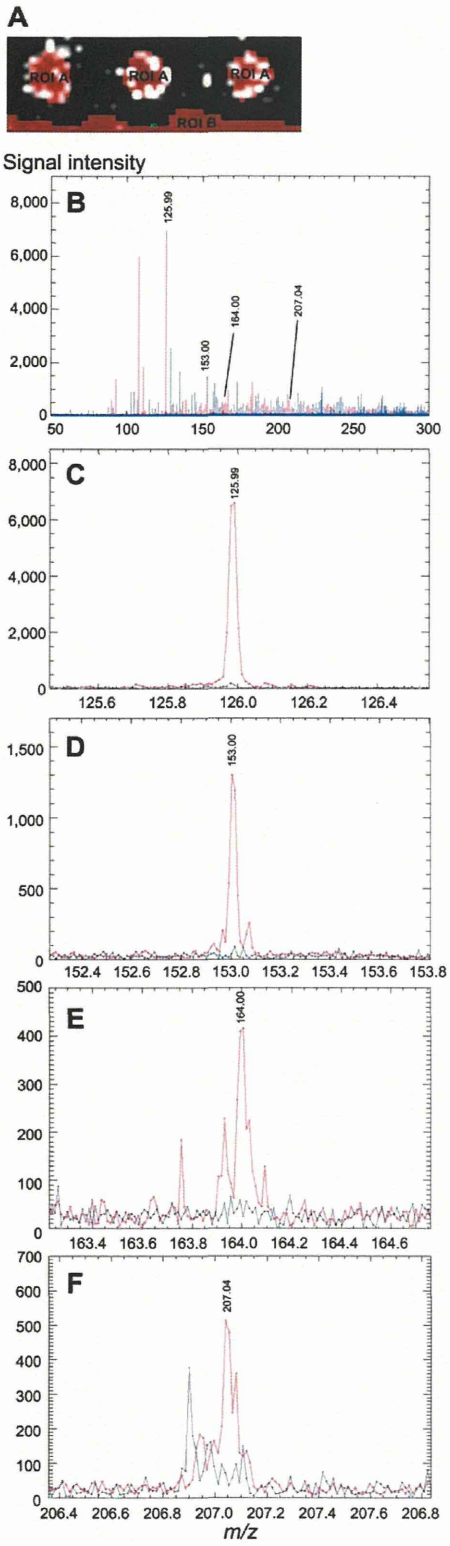

Fig. 4. Hair-Specific Mass Spectra of Putative Aging Markers

ROI-specific mass spectra in subject No. 1 are presented. Red peaks and blue peaks are derived from the hair section and background area, respectively. (A) ROI selection is illustrated: ROI A as hair section and ROI B as background area. (B) *m/z* 50 to 300. (C) *m/z* 125.99. (D) *m/z* 153.00. (E) *m/z* 164.00. (F) *m/z* 207.04. (Reprinted from ref. 68 with permission from The Public Library of Science.)

tissue microarray to study gastric carcinoma tissue samples by IMS, and successfully identified histone (H4)-specific signals in poorly differentiated cancer tissue samples by utilizing tandem MS.[63] Proteomic-based IMS investigations have resulted in a better understanding of carcinogenesis, invasiveness, metastasis, and the prognosis process in gastric cancer patients.

3. DEVELOPMENT AND APPLICATION OF HIGH-RESOLUTION ATMOSPHERIC PRESSURE-LASER MASS MICROSCOPE

3.1. Development of a 'Mass Microscope' Recently, we have developed a 'mass microscope' consisting of a microscope coupled with high-resolution atmospheric pressure-laser desorption/ionization (AP-LDI) and a quadruple ion trap-time-of-flight (QIT-TOF)-analyzer[66] (Fig. 2). This instrument allows us to precisely observe a specific tissue section before IMS and analyze the biomolecules with a spatial resolution of 10 μm on the tissue section. An UV laser tightly focused with a triplet lens was used to achieve high spatial resolution. An atmospheric pressure ion-source chamber enables us to analyze fresh samples with minimal loss of intrinsic water or volatile compounds.

3.2. Analysis of Disease Biomarkers in Fabry's Disease We have used IMS to achieve the accurate diagnosis of Fabry's disease, especially in questionable cases, and have shown that IMS has a higher specificity than electron microscopy or enzyme activity assays, which are based on light microscopy. We constructed images by determining the locations of these peaks within an endomyocardial (EMB) biopsy sample.[67] We observed that the distribution of globotriaosylceramides (Gb3s) was consistent with that of cardiomyocytes, especially in areas that were affected by vacuolar degeneration, and that the Gb3 types existed together in some parts and separately in others (Figs. 3A,B). In contrast, as shown in Figs. 3C and D, Gb3 was not detected in the control EMB sample. When we analyzed the heart from a mouse with Fabry's disease, we also detected Gb3s in the cardiac tissue, even though there was no evidence of vacuolation in the cardiomyocytes on light microscopy (Figs. 3E,F). Gb3 was not detected in the control mouse heart. We could detect Gb3s not only in the heart from a Fabry's disease patient, but also in the heart from a mouse model of Fabry's disease without discernible degenerative changes on light microscopy. Although the significance of each type of Gb3 distribution is unknown, it is possible that these distribution patterns could help to distinguish variations in the disease phenotype or evaluate the effectiveness of enzyme replacement therapy, which may also help to elucidate the basis for the disease. However, this issue requires further study. The current study presents novel findings suggesting that IMS is useful for diagnosing Fabry's disease with cardiac manifestations, especially in questionable cases. Because IMS can directly analyze the molecular weight of each existing component, IMS has a higher specificity than electron microscopy or enzyme activity assays when Fabry's disease is suspected based on light microscopy. Our results indicate that IMS is a new tool that can be used to accurately diagnose not only Fabry's disease, but also other unknown storage diseases.

3.3. Analysis of Biomolecules in Human Hair The mass microscope has a subcellular spatial resolution of 10 μm for the detection of molecules from a tissue section. We have

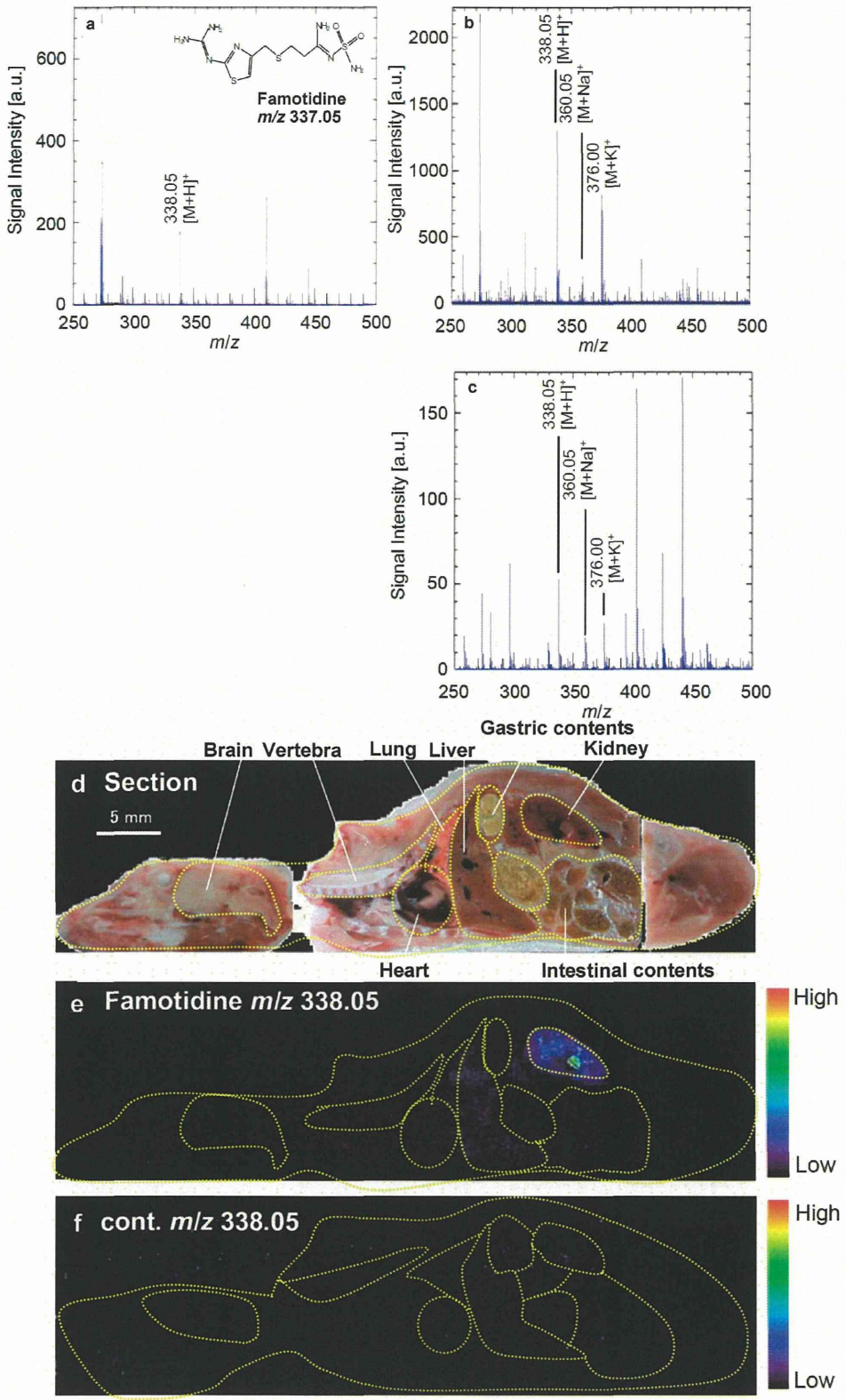

Fig. 5. Mass Spectrum of Famotidine and an MS Ion Image of a Whole-Body Section

(A) Structure and mass spectrum of famotidine. (B) Mass spectrum of famotidine detected in a tissue section. (C) Mass spectrum of famotidine detected in the kidney in a tissue section. (D) Optical image of a mouse tissue section. (E) MS ion image of famotidine (*m/z* 338.05) on a mouse tissue section 3 min after injection. Famotidine is localized to a significant extent in the kidney. (F) MS ion image at *m/z* 338.05 on a control mouse tissue section. (Reprinted from ref. 69 with permission from Journal of the Mass Spectrometry Society of Japan.)

applied this system to analyze human hair cross sections, and have detected biomolecules showing aging-related alterations. The optical images obtained at high resolution showed molecular distribution in the cortex and medulla region of hair.[68] Among the 31 molecules detected specifically in hair sections, dihydrouracil and 3,4-dihydroxymandelic acid (DHMA), which are metabolites of uracil and catecholamines, respectively, exhibited a higher signal intensity in the young group than in the old, and *O*-phosphoethanolamine displayed a higher intensity in the old group (Fig. 4). Among the 3, putative *O*-phosphoethanolamine showed a cortex-specific distribution, and exhibited changes in signal intensity with aging, whereas the molecules in medulla did not exhibit significant changes.

3.4. Analysis of Drug Distribution Imaging of drugs and metabolites by MALDI-IMS offers a unique opportunity to identify changes in the distribution of a desired compound in different regions of a tissue of interest, and this technique can help us to understand whether an exogenous compound administered orally affects endogenous metabolites. Antipsychotic, cancer, anti-anxiety, and hypnotic drugs have been studied in different tissue sections by IMS to determine the distribution of molecules.[43] In these assays, a multivariate approach with MALDI-IMS is useful to investigate the dynamics of metabolites.[44] Recently, we attempted to visualize the distribution of famotidine with a higher spatial resolution in whole body mouse sections using the mass microscope that we developed, and observed famotidine was mainly distributed in the kidney (Fig. 5).[69] Moreover, a higher spatial-resolution analysis revealed that the distribution of famotidine was in the renal pelvis of the kidney. The results suggest that famotidine is concentrated in the renal pelvis through the cortex and marrow in the kidney during the excretion process. It can therefore be concluded that the mass microscope permits deeper insight into therapeutic and toxicological processes associated with drug administration.

4. FUTURE PERSPECTIVES

Many great advances have been made in MALDI-IMS to resolve molecular species in various types of biological samples, but there is still room for improvement with respect to sample preparation, ionization, and instrumentation. The mass microscope could be a powerful tool for obtaining high resolution of biomolecules in tissue samples. The fundamental contributions of MALDI-IMS will provide a powerful tool for the early detection and characterization of cellular processes in both healthy and disease conditions, and help us to understand and treat disorders very effectively.

Acknowledgments This review was undertaken on behalf of The Pharmaceutical Society of Japan for Awarding the Promotion Prize to M.S. for the development and application of IMS techniques and mass microscope. We would like to acknowledge the collaboration of past and present colleagues in the Department of Cell Biology and Anatomy of Hamamatsu University School of Medicine, Shimadzu Corporation, and many other collaborators for their work that was reviewed in this paper and supported mainly by the Japanese Science and Technology Agency (JST) in the form of a Grant-in-Aid for SENTAN.

REFERENCES

1) Kevles B. *Naked to the Bone: Medical Imaging in the Twentieth Century.* Rutgers University Press, New Brunswick, New Jersey, 1997.
2) Weissleder R, Moore A, Mahmood U, Bhorade R, Benveniste H, Chiocca EA, Basilion JP. *In vivo* magnetic resonance imaging of transgene expression. *Nat. Med.*, **6**, 351–355 (2000).
3) Setou M, Radostin D, Atsuzawa K, Yao I, Fukuda Y, Usuda N, Nagayama K. Mammalian cell nano structures visualized by cryo Hilbert differential contrast transmission electron microscopy. *Med. Mol. Morphol.*, **39**, 176–180 (2006).
4) Phelps ME, Hoffman EJ, Mullani NA, Ter-Pogossian MM. Application of annihilation coincidence detection to transaxial reconstruction tomography. *Journal of Nuclear Medicine*, **16**, 210–224 (1975).
5) Ikegami K, Heier RL, Taruishi M, Takagi H, Mukai M, Shimma S, Taira S, Hatanaka K, Morone N, Yao I, Campbell PK, Yuasa S, Janke C, Macgregor GR, Setou M. Loss of alpha-tubulin polyglutamylation in ROSA22 mice is associated with abnormal targeting of KIF1A and modulated synaptic function. *Proc. Natl. Acad. Sci. U.S.A.*, **104**, 3213–3218 (2007).
6) Yao I, Takagi H, Ageta H, Kahyo T, Sato S, Hatanaka K, Fukuda Y, Chiba T, Morone N, Yuasa S, Inokuchi K, Ohtsuka T, Macgregor GR, Tanaka K, Setou M. SCRAPPER-dependent ubiquitination of active zone protein RIM1 regulates synaptic vesicle release. *Cell*, **130**, 943–957 (2007).
7) Hatanaka T, Hatanaka Y, Setou M. Regulation of amino acid transporter ATA2 by ubiquitin ligase Nedd4-2. *J. Biol. Chem.*, **281**, 35922–35930 (2006).
8) Ikegami K, Mukai M, Tsuchida J, Heier RL, Macgregor GR, Setou M. TTLL7 is a mammalian beta-tubulin polyglutamylase required for growth of MAP2-positive neurites. *J. Biol. Chem.*, **281**, 30707–30716 (2006).
9) Hatanaka T, Hatanaka Y, Tsuchida J-i, Ganapathy V, Setou M. Amino acid transporter ATA2 is stored at the *trans*-Golgi network and released by insulin stimulus in adipocytes. *J. Biol. Chem.*, **281**, 39273–39284 (2006).
10) Konishi Y, Setou M. Tubulin tyrosination navigates the kinesin-1 motor domain to axons. *Nat. Neurosci.*, **12**, 559–567 (2009).
11) Yang HJ, Takagi H, Konishi Y, Ageta H, Ikegami K, Yao I, Sato S, Hatanaka K, Inokuchi K, Seog DH, Setou M. Transmembrane and ubiquitin-like domain-containing protein 1 (Tmub1/HOPS) facilitates surface expression of GluR2-containing AMPA receptors. *PLoS ONE*, **3**, 1–13 (2008).
12) Fukuda Y, Kawano Y, Tanikawa Y, Oba M, Koyama M, Takagi H, Matsumoto M, Nagayama K, Setou M. *In vivo* imaging of the dendritic arbors of layer V pyramidal cells in the cerebral cortex using a laser scanning microscope with a stick-type objective lens. *Neurosci. Lett.*, **400**, 53–57 (2006).
13) Asai S, Takamura K, Suzuki H, Setou M. Single-cell imaging of c-fos expression in rat primary hippocampal cells using a luminescence microscope. *Neurosci. Lett.*, **434**, 289–292 (2008).
14) Setou M, Seog D-H, Tanaka Y, Kanai Y, Takei Y, Kawagishi M, Hirokawa N. Glutamate-receptor-interacting protein GRIP1 directly steers kinesin to dendrites. *Nature*, **417**, 83–87 (2002).
15) Luxembourg SL, Mize TH, McDonnell LA, Heeren RMA. High-spatial resolution mass spectrometric imaging of peptide and protein distributions on a surface. *Anal. Chem.*, **76**, 5339–5344 (2004).
16) Brotherton HO, Yost RA. Determination of drugs in blood serum by mass spectrometry/mass spectrometry. *Anal. Chem.*, **55**, 549–553 (1983).
17) Johnson JV, Yost RA, Faull KF. Tandem mass spectrometry for the trace determination of tryptolines in crude brain extracts. *Anal. Chem.*, **56**, 1655–1661 (1984).
18) Bernier UR, Kline DL, Barnard DR, Schreck CE, Yost RA.

Analysis of human skin emanations by gas chromatography/mass spectrometry. 2. Identification of volatile compounds that are candidate attractants for the yellow fever mosquito (*Aedes aegypti*). *Anal. Chem.*, **72**, 747–756 (2000).
19) Garrett TJ, Yost RA. Analysis of intact tissue by intermediate-pressure MALDI on a linear ion trap mass spectrometer. *Anal. Chem.*, **78**, 2465–2469 (2006).
20) Rubakhin SS, Greenough WT, Sweedler JV. Spatial profiling with MALDI MS: distribution of neuropeptides within single neurons. *Anal. Chem.*, **75**, 5374–5380 (2003).
21) Rubakhin SS, Churchill JD, Greenough WT, Sweedler JV. Profiling signaling peptides in single mammalian cells using mass spectrometry. *Anal. Chem.*, **78**, 7267–7272 (2006).
22) Miao H, Rubakhin SS, Sweedler JV. Subcellular analysis of D-aspartate. *Anal. Chem.*, **77**, 7190–7194 (2005).
23) Hatcher NG, Richmond TA, Rubakhin SS, Sweedler JV. Monitoring activity-dependent peptide release from the CNS using single-bead solid-phase extraction and MALDI TOF MS detection. *Anal. Chem.*, **77**, 1580–1587 (2005).
24) Sugiura Y, Shimma S, Setou M. Two-step matrix application technique to improve ionization efficiency for matrix-assisted laser desorption/ionization in imaging mass spectrometry. *Anal. Chem.*, **78**, 8227–8235 (2006).
25) Shimma S, Furuta M, Ichimura K, Yoshida Y, Setou M. A novel approach to *in situ* proteome analysis using chemical inkjet printing technology and MALDI-QIT-TOF tandem mass spectrometer. *Journal of the Mass Spectrometry Society of Japan*, **54**, 133–140 (2006).
26) Shimma S, Furuta M, Ichimura K, Yoshida Y, Setou M. Direct MS/MS analysis in mammalian tissue sections using MALDI-QIT-TOF-MS and chemical inkjet technology. *Surf. Interface Anal.*, **38**, 12–13, 1712–1714 (2006).
27) Chaurand P, Schwartz SA, Reyzer ML, Caprioli RM. Imaging mass spectrometry: principles and potentials. *Toxicol. Pathol.*, **33**, 92–101 (2005).
28) Stoeckli M, Chaurand P, Hallahan DE, Caprioli RM. Imaging mass spectrometry: a new technology for the analysis of protein expression in mammalian tissues. *Nat. Med.*, **7**, 493–496 (2001).
29) Sugiura Y, Shimma S, Moriyama Y, Setou M. Direct analysis of cultured cells with matrix-assisted laser desorption/ionization on conductive transparent film. *Journal of the Mass Spectrometry Society of Japan*, **55**, 25–31 (2007).
30) Chaurand P, Schriver KE, Caprioli RM. Instrument design and characterization for high resolution MALDI-MS imaging of tissue sections. *J. Mass Spectrom.*, **42**, 476–489 (2007).
31) Schwartz SA, Weil RJ, Johnson MD, Toms SA, Caprioli RM. Protein profiling in brain tumors using mass spectrometry: feasibility of a new technique for the analysis of protein expression. *Clin. Cancer Res.*, **10**, 981–987 (2004).
32) Pierson J, Norris JL, Aerni HR, Svenningsson P, Caprioli RM, Andrén PE. Molecular profiling of experimental Parkinson's disease: direct analysis of peptides and proteins on brain tissue sections by MALDI mass spectrometry. *J. Proteome Res.*, **3**, 289–295 (2004).
33) Jackson SN, Wang H-YJ, Woods AS. *In situ* structural characterization of phosphatidylcholines in brain tissue using MALDI-MS/MS. *J. Am. Soc. Mass Spectrom.*, **16**, 2052–2056 (2005).
34) Jackson SN, Wang H-YJ, Woods AS, Ugarov M, Egan T, Schultz JA. Direct tissue analysis of phospholipids in rat brain using MALDI-TOFMS and MALDI-ion mobility-TOFMS. *J. Am. Soc. Mass Spectrom.*, **16**, 133–138 (2005).
35) Touboul D, Piednoël H, Voisin V, De La Porte S, Brunelle A, Halgand F, Laprévote O. Changes of phospholipid composition within the dystrophic muscle by matrix-assisted laser desorption/ionization mass spectrometry and mass spectrometry imaging. *Eur. J. Mass Spectrom.* (Chichester, Eng.), **10**, 657–664 (2004).
36) Khatib-Shahidi S, Andersson M, Herman JL, Gillespie TA, Caprioli RM. Direct molecular analysis of whole-body animal tissue sections by imaging MALDI mass spectrometry. *Anal. Chem.*, **78**, 6448–6456 (2006).
37) Takáts Z, Wiseman JM, Gologan B, Cooks RG. Mass spectrometry sampling under ambient conditions with desorption electrospray ionization. *Science*, **306**, 471–473 (2004).
38) Benninghoven A. Surface investigation of solids by the statical method of secondary ion mass spectroscopy (SIMS). *Surf. Sci.*, **35**, 427–457 (1973).
39) Tanaka K, Waki H, Ido Y, Akita S, Yoshida Y, Yoshida T, Matsuo T. Protein and polymer analyses up to *m/z* 100000 by laser ionization time-of-flight mass spectrometry. *Rapid Commun. Mass Spectrom.*, **2**, 151–153 (1988).
40) Rohner TC, Staab D, Stoeckli M. MALDI mass spectrometric imaging of biological tissue sections. *Mech. Ageing Dev.*, **126**, 177–185 (2005).
41) Shimma S, Sugiura Y, Hayasaka T, Zaima N, Matsumoto M, Setou M. Mass imaging and identification of biomolecules with MALDI-QIT-TOF-based system. *Anal. Chem.*, **80**, 878–885 (2008).
42) Sugiura Y, Konishi Y, Zaima N, Kajihara S, Nakanishi H, Taguchi R, Setou M. Visualization of the cell-selective distribution of PUFA-containing phosphatidylcholines in mouse brain by imaging mass spectrometry. *J. Lipid Res.*, **50**, 1776–1788 (2009).
43) Sugiura Y, Shimma S, Konishi Y, Yamada MK, Setou M. Imaging mass spectrometry technology and application on ganglioside study; visualization of age-dependent accumulation of C20-ganglioside molecular species in the mouse hippocampus. *PLoS ONE*, **3**, 1–9 (2008).
44) Zaima N, Matsuyama Y, Setou M. Principal component analysis of direct matrix-assisted laser desorption/ionization mass spectrometric data related to metabolites of fatty liver. *J. Oleo Sci.*, **58**, 267–273 (2009).
45) Goto-Inoue N, Hayasaka T, Zaima N, Setou M. The specific localization of seminolipid molecular species on mouse testis during testicular maturation revealed by imaging mass spectrometry. *Glycobiology*, **19**, 950–957 (2009).
46) Hayasaka T, Goto-Inoue N, Sugiura Y, Zaima N, Nakanishi H, Ohishi K, Nakanishi S, Naito T, Taguchi R, Setou M. Matrix-assisted laser desorption/ionization quadrupole ion trap time-of-flight (MALDI-QIT-TOF)-based imaging mass spectrometry reveals a layered distribution of phospholipid molecular species in the mouse retina. *Rapid Commun. Mass Spectrom.*, **22**, 3415–3426 (2008).
47) Shimma S, Sugiura Y, Hayasaka T, Hoshikawa Y, Noda T, Setou M. MALDI-based imaging mass spectrometry revealed abnormal distribution of phospholipids in colon cancer liver metastasis. *J. Chromatogr. B Analyt. Technol. Biomed. Life Sci.*, **855**, 98–103 (2007).
48) Hosokawa N, Sugiura Y, Setou M. Spectrum Normalization Method Using an External Standard in Mass Spectrometric Imaging. *Journal of the Mass Spectrometry Society of Japan*, **56**, 77–81 (2008).
49) Goto-Inoue N, Hayasaka T, Sugiura Y, Taki T, Li YT, Matsumoto M, Setou M. High-sensitivity analysis of glycosphingolipids by matrix-assisted laser desorption/ionization quadrupole ion trap time-of-flight imaging mass spectrometry on transfer membranes. *J. Chromatogr. B*, **870**, 74–83 (2008).
50) Sugiura Y, Shimma S, Setou M. Thin sectioning improves the peak intensity and signal-to-noise ratio in direct tissue mass spectrometry. *Journal of the Mass Spectrometry Society of Japan*, **54**, 45–48 (2006).
51) Taira S, Sugiura Y, Moritake S, Shimma S, Ichiyanagi Y, Setou M. Nanoparticle-assisted laser desorption/ionization based mass imaging with cellular resolution. *Anal. Chem.*, **80**, 4761–4766 (2008).
52) Moritake S, Taira S, Sugiura Y, Setou M, Ichiyanagi Y. Magnetic nanoparticle-based mass spectrometry for the detection of biomolecules in cultured cells. *J. Nanosci. Nanotechnol.*, **9**, 169–176 (2009).
53) Ageta H, Asai S, Sugiura Y, Goto-Inoue N, Zaima N, Setou M. Layer-specific sulfatide localization in rat hippocampus middle molecular layer is revealed by nanoparticle-assisted laser desorption/

ionization imaging mass spectrometry. *Med. Mol. Morphol.*, **42**, 16–23 (2009).
54) Nakagawa T, Setou M, Seog D, Ogasawara K, Dohmae N, Takio K, Hirokawa N. A novel motor, KIF13A, transports mannose-6-phosphate receptor to plasma membrane through direct interaction with AP-1 complex. *Cell*, **103**, 569–581 (2000).
55) Setou M, Nakagawa T, Seog D-H, Hirokawa N. Kinesin superfamily motor protein KIF17 and mLin-10 in NMDA receptor-containing vesicle transport. *Science*, **288**, 1796–1802 (2000).
56) Müthing J. High-resolution thin-layer chromatography of gangliosides. *J. Chromatogr. A*, **720**, 3–25 (1996).
57) van Echten-Deckert G. Sphingolipid extraction and analysis by thin-layer chromatography. *Methods Enzymol.*, **312**, 64–79 (2000).
58) Yu RK, Ariga T. Ganglioside analysis by high-performance thin-layer chromatography. *Methods Enzymol.*, **312**, 115–134 (2000).
59) Hayasaka T, Goto-Inoue N, Zaima N, Kimura Y, Setou M. Organ-specific distributions of lysophosphatidylcholine and triacylglycerol in mouse embryo. *Lipids*, **44**, 837–848 (2009).
60) Valdes-Gonzalez T, Goto-Inoue N, Hirano W, Ishiyama H, Hayasaka T, Setou M, Taki T. New approach for glyco- and lipidomics—molecular scanning of human brain gangliosides by TLC-Blot and MALDI-QIT-TOF MS. *J. Neurochem.*, **116**, 678–683 (2011).
61) Ikegami K, Horigome D, Mukai M, Livnat I, MacGregor GR, Setou M. TTLL10 is a protein polyglycylase that can modify nucleosome assembly protein 1. *FEBS Lett.*, **582**, 1129–1134 (2008).
62) Hatanaka K, Ikegami K, Takagi H, Setou M. Hypo-osmotic shock induces nuclear export and proteasome-dependent decrease of UBL5. *Biochem. Biophys. Res. Commun.*, **350**, 610–615 (2006).
63) Morita Y, Ikegami K, Goto-Inoue N, Hayasaka T, Zaima N, Tanaka H, Uehara T, Setoguchi T, Sakaguchi T, Igarashi H, Sugimura H, Setou M, Konno H. Imaging mass spectrometry of gastric carcinoma in formalin-fixed paraffin-embedded tissue microarray. *Cancer Sci.*, **101**, 267–273 (2010).
64) Yao I, Sugiura Y, Matsumoto M, Setou M. *In situ* proteomics with imaging mass spectrometry and principal component analysis in the Scrapper-knockout mouse brain. *Proteomics*, **8**, 3692–3701 (2008).
65) Setou M, Hayasaka T, Shimma S, Sugiura Y, Matsumoto M. Protein denaturation improves enzymatic digestion efficiency for direct tissue analysis using mass spectrometry. *Appl. Surf. Sci.*, **255**, 1555–1559 (2008).
66) Harada T, Yuba-Kubo A, Sugiura Y, Zaima N, Hayasaka T, Goto-Inoue N, Wakui M, Suematsu M, Takeshita K, Ogawa K, Yoshida Y, Setou M. Visualization of volatile substances in different organelles with an atmospheric-pressure mass microscope. *Anal. Chem.*, **81**, 9153–9157 (2009).
67) Onoue K, Zaima N, Sugiura Y, Isojima T, Okayama S, Horii M, Akai Y, Uemura S, Takemura G, Sakuraba H, Sakaguchi Y, Setou M, Saito Y. Using imaging mass spectrometry to accurately diagnose Fabry's disease. *Circ. J.*, **75**, 221–223 (2011).
68) Waki ML, Onoue K, Takahashi T, Goto K, Saito Y, Inami K, Makita I, Angata Y, Suzuki T, Yamashita M, Sato N, Nakamura S, Yuki D, Sugiura Y, Zaima N, Goto-Inoue N, Hayasaka T, Shimomura Y, Setou M. Investigation by imaging mass spectrometry of biomarker candidates for aging in the hair cortex. *PLoS ONE*, **6**, 1–9 (2011).
69) Saito Y, Hayasaka T, Onoue K, Takizawa Y, Kajihara S, Ogawa K, Setou M. Pharmacokinetic analysis using a high spatial-resolution mass microscope. *Journal of the Mass Spectrometry Society of Japan*, **59**, 79–84 (2011).

DOI: 10.1002/cbic.201200146

High-Resolution Multi-isotope Imaging Mass Spectrometry Enables Visualisation of Stem Cell Division and Metabolism

Kensuke Goto, Michihiko Waki, Tsukasa Takahashi, Makoto Kadowaki, and Mitsutoshi Setou*[a]

The "immortal-strand hypothesis" predicts the random segregation of chromosomes during asymmetric stem-cell division. Stem cells exhibit two cell division patterns, namely symmetric and asymmetric division. When a stem cell divides asymmetrically into two cells, it produces two different kinds of cells, namely a daughter cell that will remain a stem cell and a progenitor cell with limited self-renewal potential. During asymmetric division, the stem cell synthesises new DNA strands from the old DNA template. In this hypothesis, the parental stem cell distributes the old and new strands to the daughter and progenitor cells, respectively, so that the stem cell retains the old strand through every asymmetric division. It was proposed by John Cairns in 1975 that it is preferable for old DNA strands to be retained in parental stem cells in order to avoid any accumulation of mutations in their genome.[1]

The validity of this hypothesis has been extensively argued over a long period of time. Primary studies have examined the hypothesis in simple organisms showing asymmetric cell division, such as bacteria, plants, and fungi. An initial report on budding yeast showed, by using autoradiography, asymmetric strand segregation between parent and daughter cells.[2] This result was, however, not confirmed in subsequent fluorescence analysis of bromodeoxyuridine (BrdU) incorporation, although it must be borne in mind that different strains were used.[3] Regarding the in vivo assessment of stem cells in mammalian tissues, Potten and colleagues first reported positive evidence in a stem cell population of mouse small-intestinal epithelium.[4] This assessment involved the use of DNA synthesis markers: ^{3}H-thymidine to label the oldest strands, and BrdU, to label newly synthesised strands. As shown by the authors, cells carrying both ^{3}H-thymidine and BrdU were observed in the stem-cell region soon after the administration of BrdU, whereas BrdU labelling was rapidly cleared from those cells that continued to retain ^{3}H-thymidine over the next several days: this resulted in these stem cells being called label-retaining cells or LRCs. This and subsequent studies using a similar approach have been considered to provide highly supportive evidence of nonrandom template-strand segregation; LRCs in the mouse mammary gland were shown to divide while retaining their old template DNA strands labelled with ^{3}H-thymidine.[5] Adult muscle satellite cells, which possess stem-cell-like properties, were shown to have an LRC subpopulation in vivo.[6] Neural stem cells labelled with BrdU showed retention of the BrdU signal after division in vitro.[7] On the other hand, asymmetric segregation of chromosomes has not been confirmed in haematopoietic stem cells in vitro or in vivo, thus indicating that asymmetric segregation is not a general property of stem cells.[8]

In ■■a new *OK?*■■ study, the authors used the powerful technique of multi-isotope imaging mass spectrometry (MIMS) to provide evidence that chromosomes are randomly segregated into two kinds of cells during asymmetric stem cell division.[9] MIMS offers unique capabilities for isotopic measurement and imaging (down to 50 nm lateral resolution), which, combined with an isotopic (or elemental) labelling strategy, allows biologists to view and quantify turnovers and to follow the fate of biomolecules with a resolution sufficient for the observation of intracellular compartments. The technique is based essentially on secondary ion-microprobe mass spectrometry (SIMS; Figure 1 A).[10] SIMS is a classical ionisation method that utilises an ion beam as a means of sputtering molecules onto samples. The ion beam is so strong that molecules on tissues are disrupted to the level of atoms. Thus, the MIMS system uses SIMS to detect sputtered atoms according to their mass. Therefore, MIMS achieves several key features simultaneously, including high spatial resolution, high sensitivity, high mass resolution, parallel acquisition of masses (seven molecular species at most) and fast acquisition of ions. Acquired data on multiple planes are compressed to form a single mass image in order to reduce matrix effects and to increase the number of counts of secondary ions (Figure 1 B). Mass images obtained for two species of atoms are used to form a hue-saturation image, a representation of the isotope ratio within a sample (Figure 1 C). Furthermore, thanks to recent improvements, isotope ratio reproducibility of a few tenths per ■■million *OK?* ■■ can now be achieved.

The technique was first termed MIMS in 2004[11] and has been applied to cultured cells, human hair and bacteria.[12] In human hair, the elemental compositions of melanin granules and other components of the hair shaft were determined by observing naturally occurring atoms such as ^{16}O, ^{14}N and ^{32}S. In addition, recent application of the technique in bacteria has

[a] *K. Goto, Dr. M. Waki, T. Takahashi, M. Kadowaki, Prof. Dr. Dr. M. Setou*
Department of Cell Biology and Anatomy
Hamamatsu University, School of Medicine
1-20-1 Handayama, Hamamatsu, Shizuoka 431-3192 (Japan)
E-mail: setou@hama-med.ac.jp

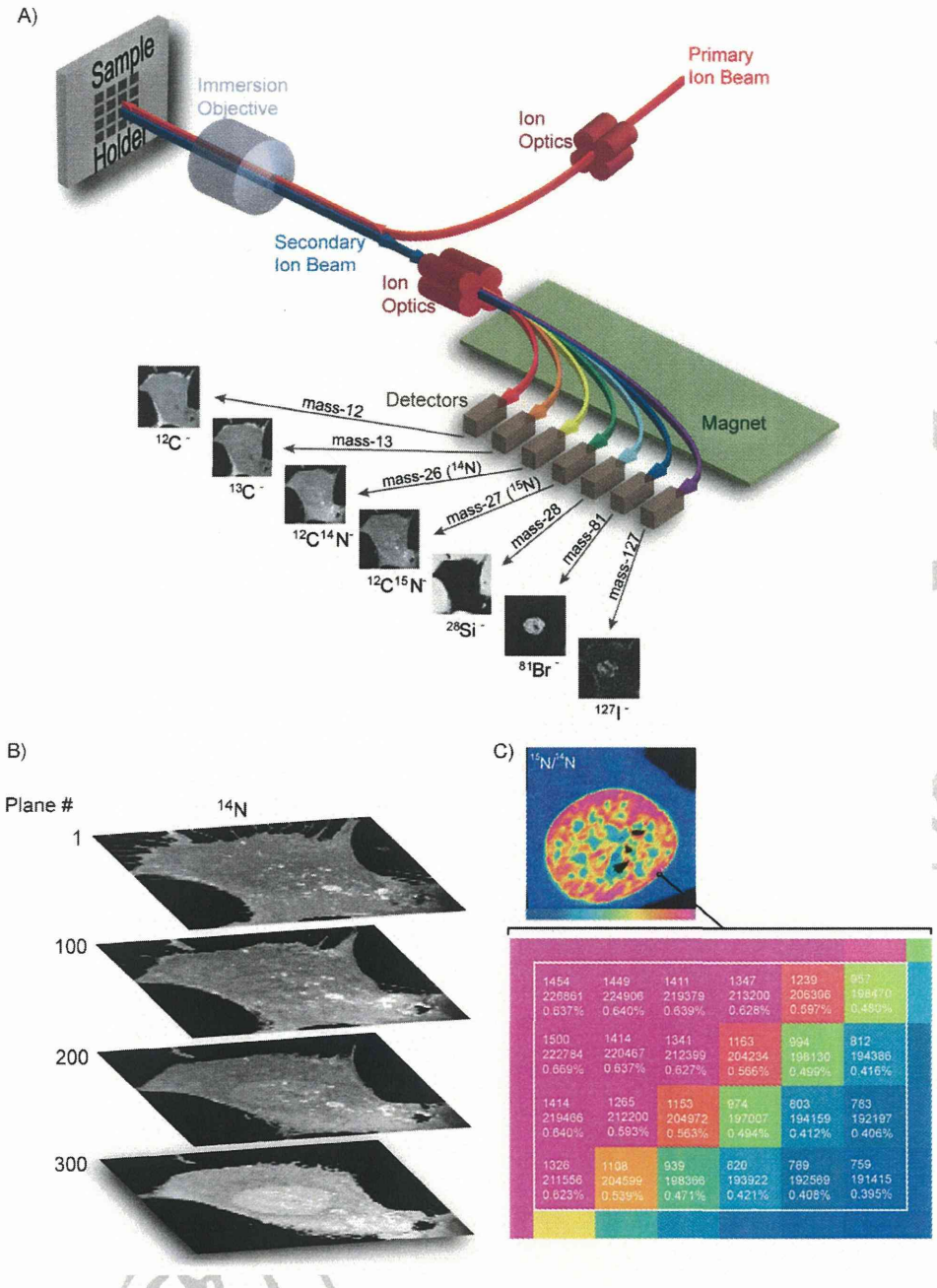

Figure 1. Multi-isotope imaging mass spectrometry (MIMS). A) Schematic depiction of the MIMS method. B) Ion images of successive planes acquired at the same location. Many successive planes can be compressed to form a single image so as to reduce errors. C) A quantitative ratio image—a hue-saturation image—can be obtained by comparing the quantitative data from two different masses. Reprinted by permission from Macmillan Publishers Ltd. from ref. [9], copyright: 2012.

enabled direct imaging and measurement of nitrogen fixation and metabolism.[12e,13]

The advantages of MIMS compared with conventional methods for detecting nucleic acid metabolism are as follows: 1) MIMS can detect ^{14}N and ^{15}N as the recombinant ion ■■CN^- *or* CN– *?*■■ to visualise nucleic acids, thus enabling simultaneous imaging of the newly synthesised DNA strand labelled with ^{15}N and the intact strand containing ^{14}N. This feature enables strict evaluation of the presence/absence of daughter strands. 2) The NanoSIMS 50 can be used to localise simultaneously two isotopes of the same element, thus avoiding artefacts due to matrix effects, and allowing unmodified molecules to be studied rather than modified ones such as BrdU, the distribution of which can also be determined by this technique. Therefore it enables critical comparison of the location of ^{14}N/^{15}N-labelled and BrdU-labelled chromosomes.

First, the authors confirmed that the technique they established is useful for the detection and quantification of ^{15}N incorporated into cells in vitro and in vivo. They supplemented a medium containing dividing fibroblasts with ^{15}N-thymidine or ■■and*?*■■ injected it into the venous blood of mice by using surgically implanted osmotic minipumps. Then, they collected jejunal segments from the mice and fixed them. After fixation, the tissues were embedded, sectioned at a thickness of 0.5 μm, and mounted on silicon chips. Thus, the atoms in the small intestine of mice were visualised, and the incorporation of ^{15}N-thymidine was quantified.

Then they used the MIMS technique to validate the immortal-strand hypothesis in the small intestine of the mouse at two different stages. They injected ^{15}N-thymidine into mice for eight weeks after birth; this allowed developmental stem cells to incorporate ^{15}N-thymidine into their own DNA strands. A four-week chase was performed after adding the ^{15}N-thymidine. Finally, they labelled proliferating cells, including stem cells, with BrdU and observed the results by using MIMS. If the hypotheses were correct, stem cells would retain the labelled thymidine in their template strands through every asymmetric division. However, the results showed no ^{15}N signals in the area where the existence of stem cells was expected based on the anatomical relationship with Paneth cells, which can be identified by their granules. If chromosomes containing ^{15}N-

thymidine were equally segregated, the signal intensity of ^{15}N would halve. Therefore, these data suggest that ^{15}N-thymidine in DNA was diluted during every asymmetric division, that is, the hypothesis is incorrect.

In their next experiment, the authors injected ^{15}N-thymidine into mice with mature stem cells. After formation, stem cells incorporate ^{15}N-thymidine into the newly synthesised DNA strands during asymmetric division and, therefore, do not retain ^{15}N-thymidine in their old DNA strands, as based on the hypothesis. Two weeks after the administration of ^{15}N-thymidine, the authors labelled proliferating cells, including stem cells, with BrdU and observed the results by using MIMS. The results showed that all proliferating cells (BrdU+) exhibited ^{15}N signals. Thus, stem cells retain ^{15}N-thymidine in their DNA strands. From these data obtained during the two different stages of stem cells, the authors confirmed the random segregation of chromosomes during asymmetric division.

Finally, the authors introduced the use of MIMS for *Drosophila* and human cells, and demonstrated its utility in these applications. *Drosophila* is useful for genetic analysis of the metabolism of lipids, ■■the distribution of lipids in *Drosophila* having been studied *OK?*■■ in an in vitro system.[14] In the animal ■■insect *?*■■ model, adipose accumulates in the fat body, which is a unique tissue; many studies have analysed the regulation of adipose in this tissue. It was found that many genes that function in the fat body are conserved in both humans and *Drosophila*. In order to confirm the high resolution of MIMS, the authors used *Drosophila* as an example and visualised lipid metabolism. They labelled palmitate with ^{13}C, and observed cells in the gut and fat body of *Drosophila*. The data show a difference in the amount of ^{13}C-palmitate incorporation between cell types in these two organs; this is consistent with the organs' functions, namely absorption and major lipid storage, respectively. The authors also observed the amount of ^{13}C-palmitate decay in the gut, it was estimated that a high frequency of lipid turnover would be exhibited. The findings revealed that decay followed an exponential curve, with a half-time of approximately 9 h. Moreover, this study assessed, for the first time, the application of MIMS in humans. The authors administered ^{15}N-thymidine to volunteers by intravenous infusion and observed peripheral white blood cell smears. They found no labelled white blood cells immediately after infusion; however, they found a few labelled cells after a four-week chase. The lag time is consistent with the time it takes to release the cells from the bone marrow.

The results presented in the article by Steinhauser and co-workers are quite significant because: 1) they prove that MIMS can be used for the quantitative analysis of metabolism in living mammalian bodies; 2) they provide strong evidence to negate the hypothesis of asymmetric segregation of chromosomes in stem cells in the small intestine; and 3) they confirm that MIMS following isotope labelling can be used to analyse nucleic acids in live organisms including mammals.[15] In particular, Figure 4 of the article shows the first application of isotope labelling to live humans and subsequent MIMS analysis of cells in the peripheral blood.[9]

The asymmetric segregation of chromosomes in stem cells has been examined in many locations other than the small intestine, including the muscle, breast, brain and blood. As indicated above, the different experimental methodologies used in these studies hinder any strict comparison of results or elucidation of the universal validity of the immortal-strand hypothesis. Utilising MIMS for the assessment of stem cells in these organs will provide evidence for clarifying this hypothesis. Here, the authors have utilised the highest available spatial resolution among the reported applications of MIMS to identify the intracellular localisation of incorporated substrates at the whole-chromosomal level. Further improvements in spatial resolution will enable the visualisation of molecules at a particular location and the microstructure of the chromosomes.[16] Such visualisation may reveal the site-specificity of transcription or replication on particular chromosomes. The authors have identified the subcellular features of metabolism mainly by visualising chromosomes, lipid droplets and actin filaments; this has resulted in the simultaneous publication of two papers in the same issue of *Nature*.[9,17] Based on these findings, the subcellular compartments analysed could be extended to other compartments such as the endoplasmic reticulum, Golgi body, proteasomes and mitochondria. As some of these compartments are segregated and reconstructed upon cellular division, the precise visualisation of molecular turnover at these structures might provide significant information regarding the mechanisms of division. Using multiple isotope-labelled substrates might lead to more molecule-specific analysis, as this technique would enable visualisation of molecular structures composed of different molecular units, for example, the detection of particular DNA and peptide motifs.[18] This article has revealed the molecular behaviour of whole chromosomes, and MIMS could therefore be used for molecular biology assessments focusing more specifically on particular genes or proteins. Several factors might limit the detection of targeted molecules by MIMS analysis, for instance the efficacy of the incorporation of isotope-labelled substrates, the area of targeted cells in the section, the intracellular degradation of isotope-labelled substrates and unwanted incorporation of the isotopes into molecules out of the target range for visualisation, among others. Among the numerous different cells in the organisms, the authors presumably found stem cells in the small intestine, indicating that these particular cells might escape the problems associated with the technique. It could be beneficial to identify organs and cell populations that are not subject to these problems or to reduce these factors by using an exogenous agent in future studies.

In conclusion, Steinhauser and co-workers have established a methodology for visualising the physiological metabolism of live mammalian organisms and provided evidence to negate the theory of asymmetric chromosomal division of stem cells in the mammalian small intestine by using this method. The methodology described in this work has the potential to be applied to unlimited experimental targets; thus, future reports published by these authors are expected to extend our biological insight further.

Keywords: asymmetric division · multi-isotope imaging mass spectrometry · chromosomes · stem cells · thymidine

[1] J. Cairns, *Nature* **1975**, *255*, 197–200.
[2] D. H. Williamson, D. J. Fennell in *Molecular Genetics in Yeast* (Eds.: D. von Wettstein, J. Friis, M. Kielland-Brandt, M. Stenderup), Alfred Benson Symposium, Munksgaard, Copenhagen, **1981**, pp. 89–107.
[3] M. W. Neff, D. J. Burke, *Genetics* **1991**, *127*, 463–473.
[4] a) C. S. Potten, W. J. Hume, P. Reid, J. Cairns, *Cell* **1978**, *15*, 899–906; b) C. S. Potten, G. Owen, D. Booth, *J. Cell Sci.* **2002**, *115*, 2381–2388.
[5] G. H. Smith, *Development* **2005**, *132*, 681–687.
[6] V. Shinin, B. Gayraud-Morel, D. Gomes, S. Tajbakhsh, *Nat. Cell Biol.* **2006**, *8*, 677–687.
[7] P. Karpowicz, C. Morshead, A. Kam, E. Jervis, J. Ramunas, V. Cheng, D. van der Kooy, *J. Cell Biol.* **2005**, *170*, 721–732.
[8] M. J. Kiel, S. He, R. Ashkenazi, S. N. Gentry, M. Teta, J. A. Kushner, T. L. Jackson, S. J. Morrison, *Nature* **2007**, *449*, 238–242.
[9] M. L. Steinhauser, A. P. Bailey, S. E. Senyo, C. Guillermier, T. S. Perlstein, A. P. Gould, R. T. Lee, C. P. Lechene, *Nature* **2012**, *481*, 516–519.
[10] a) R. Castaing, G. Slodzian, *J. Microsc.* **1962**, *1*, 395–410; b) J. L. Guerquin-Kern, F. Hillion, J. C. Madelmont, P. Labarre, J. Papon, A. Croisy, *Biomed. Eng.* **2004**, *3*, 10; c) A. Gojon, N. Grignon, P. Tillard, P. Massiot, F. Lefebvre, M. Thellier, C. Ripoll, *Cell. Mol. Biol.* **1996**, *42*, 351–360; d) E. Hindie, B. Coulomb, R. Beaupain, P. Galle, *Biol. Cell* **1992**, *74*, 81–88.
[11] R. Peteranderl, C. Lechene, *J. Am. Soc. Mass Spectrom.* **2004**, *15*, 478–485.
[12] a) J. L. Guerquin-Kern, T. D. Wu, C. Quintana, A. Croisy, *Biochim. Biophys. Acta Gen. Subj.* **2005**, *1724*, 228–238; b) P. Hallegot, R. Peteranderl, C. Lechene, *J. Invest. Dermatol.* **2004**, *122*, 381–386; c) G. McMahon, H. F. Saint-Cyr, C. Lechene, C. J. Unkefer, *J. Am. Soc. Mass Spectrom.* **2006**, *17*, 1181–1187; d) C. P. Lechene, Y. Luyten, G. McMahon, D. L. Distel, *Science* **2007**, *317*, 1563–1566; e) M. R. Kilburn, D. L. Jones, P. L. Clode, J. B. Cliff, E. A. Stockdale, A. M. Herrmann, D. V. Murphy, *Plant Signaling Behav.* **2010**, *5*, 760–762.
[13] T. Li, T. D. Wu, L. Mazeas, L. Toffin, J. L. Guerquin-Kern, G. Leblon, T. Bouchez, *Environ. Microbiol.* **2008**, *10*, 580–588.
[14] M. L. Kraft, P. K. Weber, M. L. Longo, I. D. Hutcheon, S. G. Boxer, *Science* **2006**, *313*, 1948–1951.
[15] C. A. Bourgeois, R. Dennebouy, A. Gibaud, M. Gerbault-Seureau, B. Malfoy, G. Slodzian, P. Galle, B. Dutrillaux, *Chromosome Res.* **1996**, *4*, 574–582.
[16] A. Cabin-Flaman, A. F. Monnier, Y. Coffinier, J.-N. Audinot, D. Gibouin, T. Wirtz, R. Boukherroub, H.-N. Migeon, A. Bensimon, L. Jannière, C. Ripoll, V. Norris, *Anal. Chem.* **2011**, *83*, 6940–6947.
[17] D.-S. Zhang, V. Piazza, B. J. Perrin, A. K. Rzadzinska, J. C. Poczatek, M. Wang, H. M. Prosser, J. M. Ervasti, D. P. Corey, C. P. Lechene, *Nature* **2012**, *481*, 520–524.
[18] G. Legent, A. Delaune, V. Norris, A. Delcorte, D. Gibouin, F. Lefebvre, G. Misevic, M. Thellier, C. Ripoll, *J. Phys. Chem. B* **2008**, *112*, 5534–5546.

Received: March 29, 2012
Published online on ■■ ■■, 0000

MIMS visualises metabolism: A recent publication by Steinhauser and co-workers presents a novel application of multi-isotope mass spectrometry (MIMS) to visualise physiological metabolism in live mammalian organisms, and validate the 'immortal strand hypothesis' of asymmetric chromosomal division of stem cells in the small intestine.

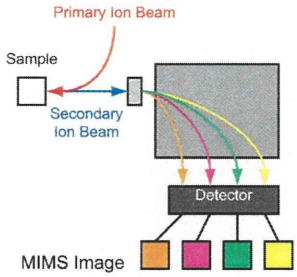

*K. Goto, M. Waki, T. Takahashi, M. Kadowaki, M. Setou**

■■ – ■■

High-Resolution Multi-isotope Imaging Mass Spectrometry Enables Visualisation of Stem Cell Division and Metabolism

3

IMAGING MASS SPECTROMETRY (IMS) FOR BIOLOGICAL APPLICATION

YUKI SUGIURA, IKUKO YAO, AND MITSUTOSHI SETOU

3.1 INTRODUCTION

3.1.1 Principle and the History of Imaging Mass Spectrometry

The development of mass spectrometry (MS) has recently entered into new paradigm. Classical matrix-assisted laser desorption/ionization (MALDI) MS has been established as an analytical method for a wide range of molecules with varied physical and chemical characteristics, and now this continuous advancing technology has been utilized into molecular imaging technique (Figure 3.1). The innovation in MS has enabled the provision of additional two-dimensional (2D) axes of recognition on tissue sections as a new approach for the life science field.

Its unique advantages, which are summarized as follows, facilitate imaging mass spectrometry (IMS) as a versatile molecular imaging technique: (1) IMS does not require any specific chemical labels or probes; (2) IMS is a "nontargeted" imaging method; and (3) the simultaneous imaging of many types of molecular species is possible. With the unique and powerful detection principle facilitated by MS, the matrix-assisted laser desorption/ionization–imaging mass spectrometry (MALDI-IMS) can be used for the visualization of the distribution of large number of biomolecules in the cells and tissues, ranging from small metabolite molecules [1,2] to much larger proteins [3,4]. Figure 3.2 illustrates the general workflow of MALDI-IMS. Basically, researchers take thin tissue slices mounted on conductive glass slides and apply a suitable MALDI matrix to the tissue section, and then the slide is inserted into a mass spectrometer. A focused laser beam is directed at predetermined positions in the tissue slice and the mass spectrometer records the spatial distribution of molecular species (typically with 10–200 μm scan pitch). Automated data collection takes 2–6 h, depending on the number of points assayed. Suitable image processing software can be used to import data from the mass spectrometer to allow visualization of ion distribution images and comparison with the histological images of the sample.

In the following sections, we will describe two major application areas: when using IMS as a technique for detection/visualization of various analytes, the application of IMS can fall roughly into two categories:

1. measurement of proteins and peptides, and
2. measurement of small organic compounds (mass-to-charge ratio [m/z] < 1000).

To date, most of the reports concerning MALDI-IMS are with regards to the detection and imaging of proteins or peptides. On the other hand, the amount of research regarding the detection/imaging of small organic molecules has been growing recently. Figure 3.3 shows the result of a PubMed search using "Imaging Mass Spectrometry" as key words (except reviews). Reports were subdivided into the two groups, according

Mass Spectrometry Handbook, First Edition. Edited by Mike S. Lee.

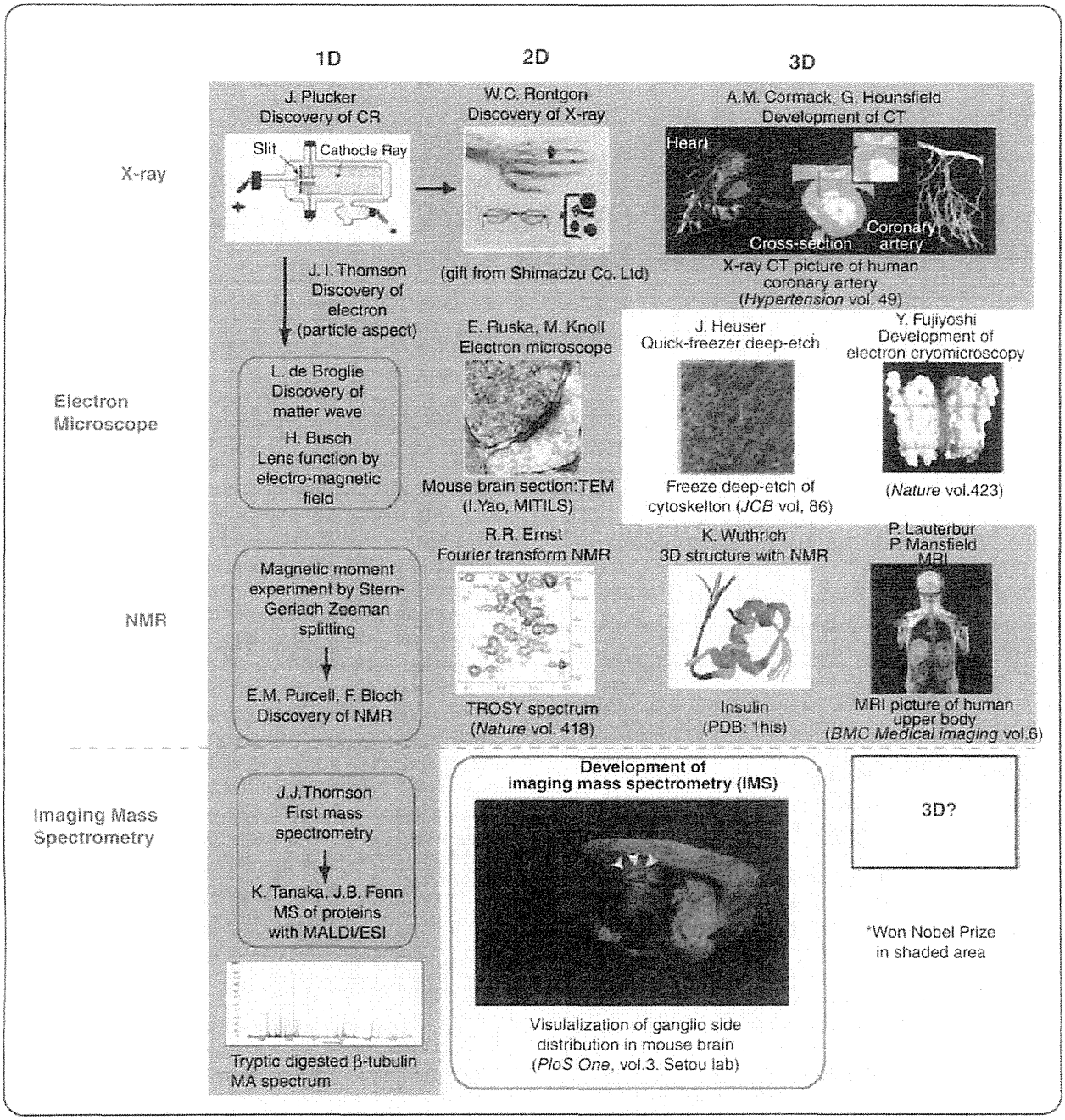

FIGURE 3.1 Historical view of the development of analytical instruments. The progress of imaging technology was categorized by its technology (longitudinal axis) and its analytical dimensions (horizontal axis). Shaded researches have received Nobel Prizes. CR, cathode ray; NMR, nuclear magnetic resonance; CT, computed tomography; TEM, transmission electron microscopy.

to the materials analyzed in the each study, and the number of reports in each group was indicated. Notably, the number of reports regarding the IMS of small compounds gradually increased and occupied half of the published work in 2007. In the following section, we shall introduce representative sample preparation strategies for analyses of distinctly structured analytes: proteins and small organic compounds, interweaving some research applications. Further, statistical analysis methods of MALDI-IMS are also described.

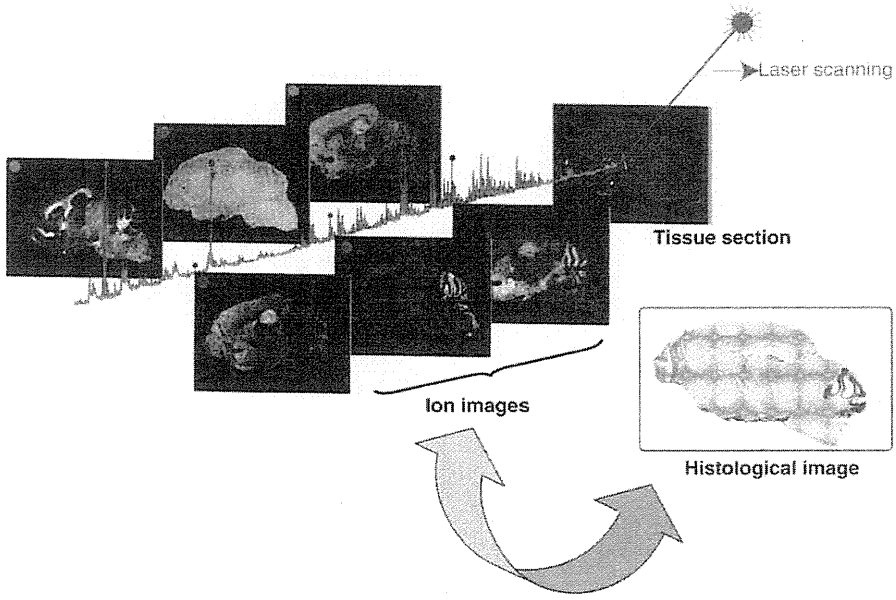

FIGURE 3.2 Schematic representations of MALDI-IMS procedures. Usually, the tissue section mounted on an indium thin oxide (ITO)-coated glass slide is covered with a specific MALDI matrix. Next, the ITO slide is inserted into a mass spectrometer. The MALDI laser scans through a set of preselected locations on the tissue (10–200 μm scan pitch) and the mass spectrometer records the spatial distribution of molecular species. Suitable image processing software can be used to import data from the mass spectrometer to allow visualization and comparison with the histological image of the sample.

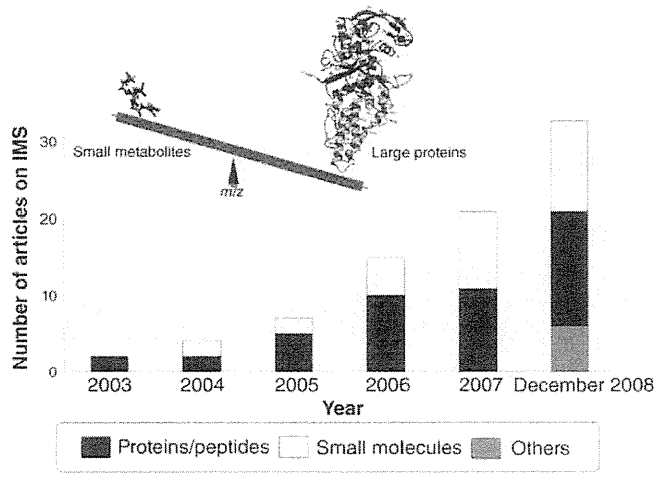

FIGURE 3.3 The result of the PubMed search using "Imaging Mass Spectrometry" as keywords.

3.2 APPLICATIONS OF MALDI-IMS

3.2.1 IMS for Proteins and Peptides

3.2.1.1 Sample Preparation Procedure for Protein Imaging In traditional MS research, analyte molecules are basically extracted and separated from crude biological samples by gas chromatography (GC) or high performance liquid chromatography (HPLC), mainly to avoid "ion suppression effect" [5–7]; in cases where such crude samples are subjected to MS, numerous molecular species compete for ionization and eventually, molecules that are easily ionized preferentially can be detected while suppressing the ionization of other molecules.

Contrastingly, in MALDI-IMS, in which the tissue sample is directly measured, researchers should pay special attention to the fact that samples are extremely complex mixtures of biomolecules. Because tissues and cells are subjected to MALDI-IMS, the sample clean-up procedure is limited. Figure 3.4 shows IMS results of spotted peptide solution (0.5 μL of 100 nM adrenocorticotropic hormone [ACTH]) on both indium tin oxide (ITO) glass slide surface and brain section, and it clearly demonstrates the severe ion suppression effect on the tissue surface; the spotted ACTH peptide was detected only from the ITO surface, but not from tissue surface. As this example indicates, an important point to consider when executing an IMS experiment is the optimization of the sample's condition, so that analyte objects can be efficiently ionized from crude mixtures.

As a practical example, when a mouse brain section to which 2,5-dihydroxybenzoic acid (DHB) has been applied as a matrix is subjected directly to MS in positive ion-detection conditions, strong peaks which are mainly derived from phospholipids were observed in mass region of $700 < m/z < 900$ [8]; on the other hand, signals derived from proteins, meanwhile, are scarcely detected at $m/z > 3000$ [9]. This is because phospholipids ionize much more efficiently than proteins, and they, on the other hand, suppress protein/peptide ionization. Therefore, for detecting/imaging proteins and peptides, removal of such lipids improves the sensitivity for proteins analysis. To this end, tissue sections should be rinsed with organic solvent, to remove lipids from tissue samples [9–11].

3.2.1.2 Rinsing of Tissue Sections: Removal of Unwanted Components As explained, the procedures of rinsing tissue sections or cells are key steps of the sample pretreatment (Figure 3.5). Such rinsing process enhances the sensitivity required for protein/peptide detection by eliminating small molecules, particularly phospholipids, from the tissues [9]. Lemaire et al. have

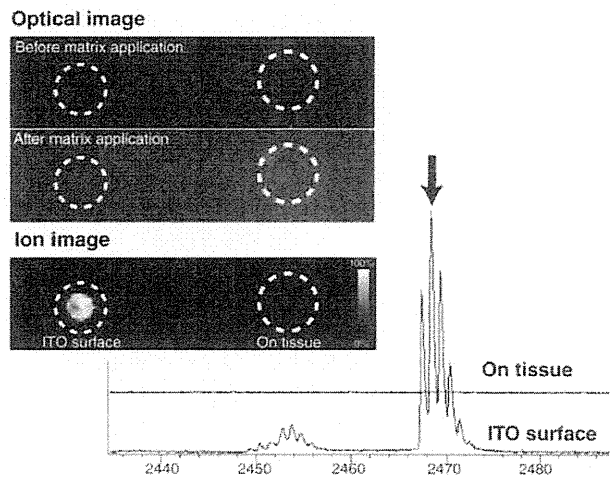

FIGURE 3.4 An example of the severe ion suppression effect on the tissue surface. A peptide solution (0.5 μL of 100 nM ACTH) was spotted on both ITO glass slide surface and brain-homogenate section. After the spraying of matrix solution (10 mg/mL α-cyano-4-hydroxycinnamic acid [α-CHCA] 50% acetonitrile, 0.1% TFA), the spotted peptide was visualized by IMS.

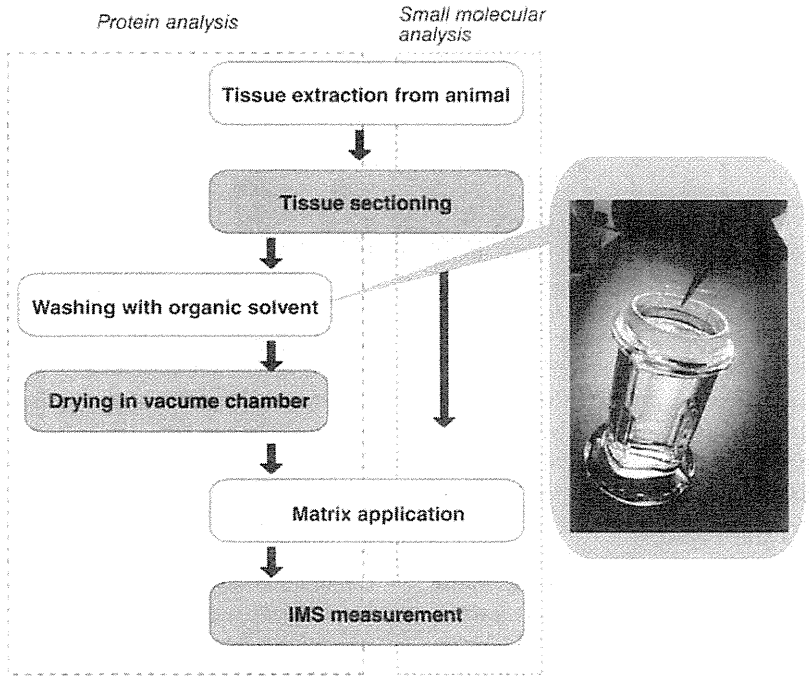

FIGURE 3.5 A scheme for protein and small molecular measurement.

examined the use of variable organic solvents in the rinsing step to enhance the efficiency of protein detection in tissue [9] (Table 3.1). They showed mass spectra obtained from mouse brain sections with or without rinsing using chloroform, acetone, or hexane, and found that the predominant signals in the vicinity of m/z 700 are abolished with rinsing procedure, and conversely, the number of peaks derived from proteins at a high molecular weight (i.e., $5000 < m/z$) increased more than 40% after rinsing. We consider that this treatment also helps remove salts, a detrimental factor that otherwise interferes with the matrix–analyte cocrystallization process and thus degrades sensitivity, particularly for large proteins, while also complicating the spectrum assignment by producing both protonated and cationated molecular ions [10].

Figure 3.6 shows an example of protein imaging in the mouse brain section. With a proper sample preparation

TABLE 3.1 The Average Number of Detected Compounds from Rat Brain Treated with Various Organic Solvents [9]

Treatment	n	Number of Detected Compounds ± Standard Deviation (%)	Increase in Detection (%)
Chloroform	10	81 ± 22	34
Hexane	5	75 ± 28	25
Toluene	5	68 ± 22	13
Xylene	5	86 ± 13	44
Acetone	5	64 ± 29	7
Untreated	10	60 ± 34	0

The average number of detected compounds and calculated increase detection for peptides/proteins of $m/z > 5000$ is determined from the mass spectra recorded on untreated rat brain sections versus organic solvent-treated ones.
n, number of experiments.

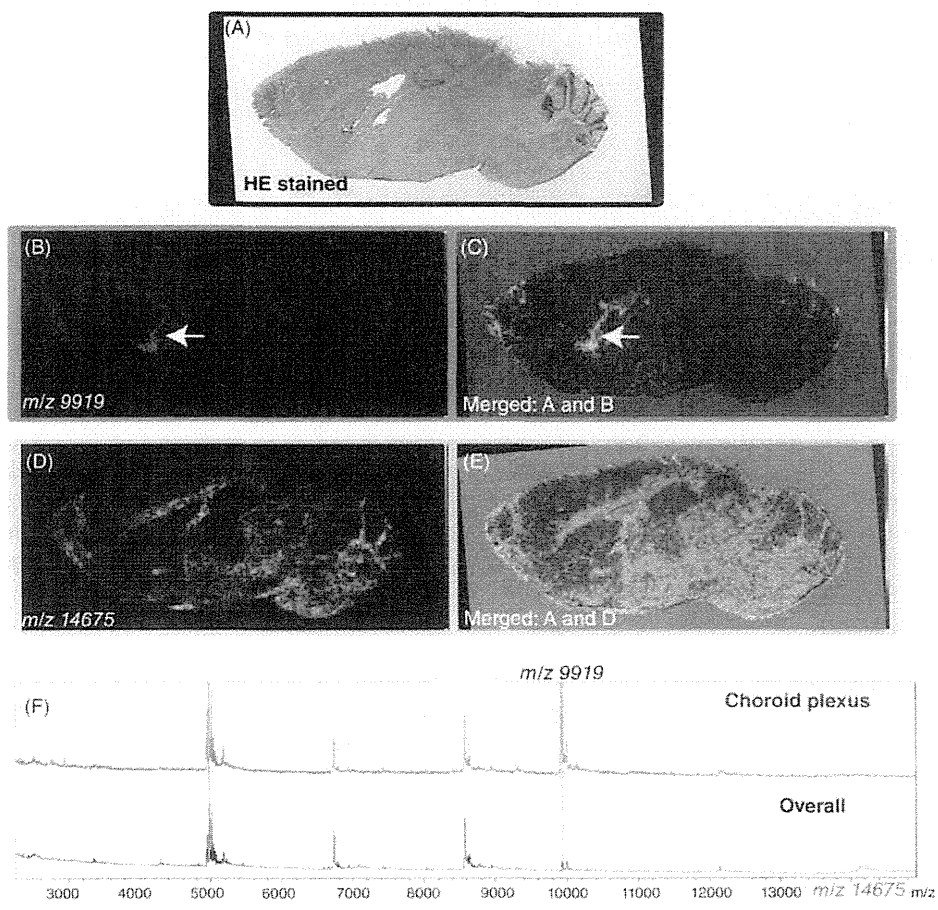

FIGURE 3.6 With proper sample preparation procedure, IMS facilitates simultaneous imaging of multiple proteins in a single tissue section. The figure shows the ion distribution images for mass peaks at m/z 9919 (B) and 14675 (D), and a microscopic observation of the same mouse brain section stained with HE after IMS measurement (C and E). The ion at m/z 14675 was localized in the white matter region, while m/z 9919 was found in choroid plexus (B and C). Averaged mass spectra from the choroid plexus and entire brain region (overall) were also presented (F).

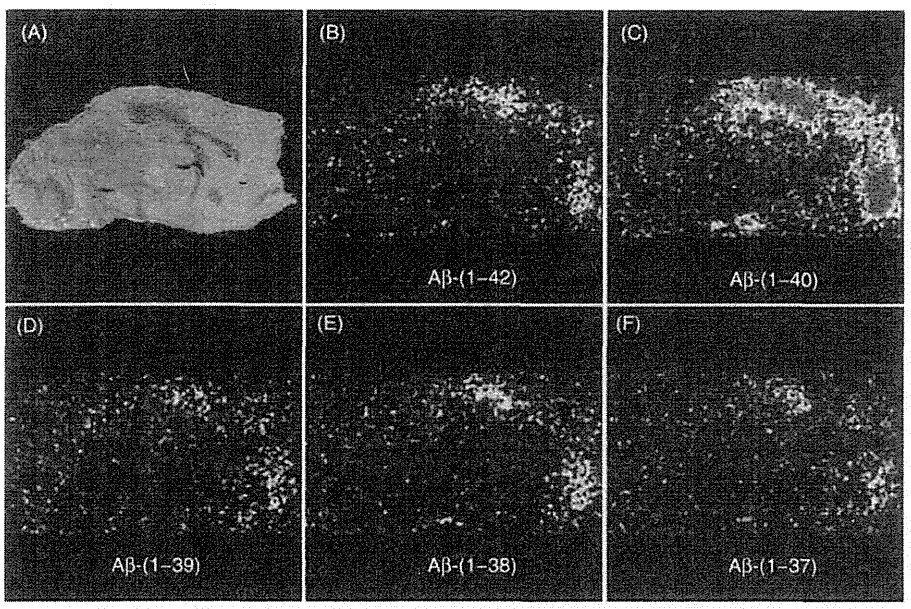

FIGURE 3.7 Distribution of six amyloid β variants in the tissue prepared from a mouse model of Alzheimer's disease. A. Optical image of the sagittal AD brain section. B–F. The molecular images of *m/z* 4515, 4330.9, 4231.7, 4132.6, and 4075.5 shows the distribution of Aβ-(1-42), Aβ-(1-40), Aβ-(1-39), Aβ-(1-38), and Aβ-(1-37), respectively [14].

procedure shown in Figure 3.5, MALDI-IMS provides simultaneous imaging of multiple proteins in a single tissue section at a time. We additionally note that researchers can histochemically stain the tissue sections which are measured by IMS after removal of the matrix and fixation procedure (in this case, immersed in methanol for 5 min). As can be seen in Figure 3.6, in conjunction with traditional light-microscopic histochemical observation, ion distribution images obtained by IMS provides valuable information regarding molecular distribution; this example demonstrates that ion at *m/z* 9919 is a specific protein expressed by cells of choroid plexus, while *m/z* 14675 is localized in the white matter region of the brain.

3.2.1.3 Application of Protein Imaging to Disease Model Mice One of the advantages of traditional MS, including both MALDI- and ESI-MS, is that they can distinguish even slight structural variations of analyte molecules by their masses. Due to this unique advantage, MS has frequently been applied to the identification/characterization of posttranslational modifications in modern proteome researches [12]. In this context, IMS also enables the distinct detection of the protein molecular species as well as the visualization of the distribution of these species on the tissue sections. As an excellent example, in the Stoeckli et al. study, amyloid β molecular species were visualized, which is generated by cleaving the amyloid precursor protein at a different cleavage site [13]. They revealed the distinct distribution of five amyloid β variants in the brain sections prepared from a mouse model of Alzheimer's disease [3,14] (Figure 3.7).

From the analytical aspect, while traditional and well-established immunohistochemistry technique requires specific antibodies which recognize each protein variant, and generation of such antibodies is a quite time-consuming procedure, on the other hand, IMS could determine the distribution of protein molecular variants at once, even *via* a simple protocol.

3.2.1.4 On-Tissue Digestion Method Traditional MALDI is used to generate intact molecular ions of proteins up to *m/z* 100,000. In the current IMS technology, however, the upper mass limit of protein detection is approximately 40 kDa because the detection sensitivity severely falls at higher mass [15]. This is a considerable limitation which narrows the application capability of this technology. As another important problem, insoluble proteins to the matrix solution, such as membrane proteins, which is a protein molecule that is attached to the membranes, are difficult to be extracted into the applied matrix solutions and thus hardly crystallize with matrix, and they were in turn difficult to detect. On this

regard, on-tissue digestion method in which proteins are denatured and enzymatically digested has been developed as an effective solution for these problems [16–18]. In this method, by cleaving large proteins, such proteins can be measured as digested proteins which are observed mainly in the mass range of $900 < m/z < 3000$. The protein digestion process also makes it easier to perform tandem mass spectrometry (MS/MS), thus to identify the molecular species directly on the tissue section [16,18] (Figure 3.8). For all these reasons, on-tissue digestion is an attractive alternative method for detecting proteins that cannot be ionized by standard methods. We previously studied this method and found that this process was enhanced by a heat-denaturation process (80°C, for 10 h) and the use of a detergent-supplemented trypsin solution (200 mg/mL trypsin in 25 mM $NH4HCO_3$ and 20 mM n-octylglucoside) (Figure 3.9; see detail protocol for Setou et al. [19]).

3.2.2 IMS for Small Organic Compounds

3.2.2.1 Employment of Optimized Experimental Protocols Is an Essential Issue In the field of the molecular biology, localization of transcripts is visualized with oligonucleotide probe in situ hybridization, and localization of proteins is visualized using immunohistochemistry based on antibodies. The emergence and continuous development of IMS could add another standard imaging technique for metabolites, whereas we do not have an established visualization technology for them. In fact, until today, the small metabolites (i.e., $m/z < 1000$) have been intensively investigated by IMS and this research application can be further subdivided into two distinct areas: (1) measurement of endogenous small organic compounds and (2) measurement of exogenous compounds (such as administrated drugs). For both, the nature of MS-based detection principle facilitates the IMS as an effective imaging tool for these metabolites in which any chemical labels and probes are not required. Such uniqueness of IMS provides a capability for simultaneous visualization of multiple metabolites, enabling to follow molecular conversion of these small organic compounds (i.e., metabolism itself) between times or conditions (Table 3.2). However, each of such diverse molecular species could have quite different chemical/physical properties, and therefore, in practical, an optimization process of experimental protocol for each analyte is still an essential issue. As a representative example, Figure 3.10 demonstrates that concentration of the organic solvent (in this case, methanol) in the matrix solution affects the detection sensitivity of lipids and peptides. The results showed that a high composition of methanol (80%–100%) was favorable for lipid detection, while a low concentration solution (20%–40%) was favorable for the detection of peptides, indicating that lipids and peptides could be efficiently extracted from tissue sections into organic and nonorganic solvents, respectively.

Figure 3.11 summarizes such key experimental points. As a first point, we have to choose the appropriate ionization method; for the detection of small metabolites, we have alternative choices other than MALDI, such as secondary ion mass spectrometry (SIMS) [15], nanostructure-initiator mass spectrometry (NIMS) [20,21], desorption/ionization on silicon (DIOS) [22], nanoparticle-assisted laser desorptiopn/ionization (nano-PALDI) [23], and even laser desorption/ionization (LDI) [24,25]. We consider that MALDI is still the most versatile method, particularly due to the soft ionization capability of intact analyte. However, other methods each have unique advantages; for example, SIMS and nano-PALDI have achieved higher spatial resolution than conventional MALDI-IMS, and above all, these mentioned alternative methods are all matrix-free methods, and thus can exclude the interruption of the matrix cluster ion. Next, if MALDI is chosen, experimenters should choose a suitable matrix compound, solvent composition, and further matrix application method for their target analyte. All these factors are critical to obtain sufficient sensitivity because they affect efficiency of analyte extraction, condition of cocrystallization, and, above all, analyte–ionization efficiency. In addition, based on the charge state of the analyte molecule, suitable MS polarity (i.e., positive/negative ion detection mode) should be used in MS measurement. Below, we shall describe the key experimental points for MALDI-IMS applications of representative metabolites.

3.2.2.2 IMS of Endogenous Metabolites: Lipids Among the endogenous metabolites, MALDI-IMS for profiling [8,26–28] and visualizing distribution [1,29] of lipids is the best established application area. In the body, numerous lipid species play specific functional roles, for example, energy storage, structural components of cell membranes, and important signaling molecule. Such lipid species may be roughly divided into three large categories: *complex lipids*, which contains phosphate and sugars in their structures (e.g., glycerophospholipids, GPLs); *simple lipids*, which are alcohol fatty acid esters (e.g., acylglycerols); and *derived lipids*, produced via hydrolysis of the simple/complex lipids (e.g., fatty acids). Table 3.3 shows the representative application studies of MALDI-IMS for lipids, and as can be seen, explorations of complex lipids have been the most intensively performed. This may be due to their easily charged structures, for example, phosphate group in phospholipids, sialic acids in gangliosides, and sulfate

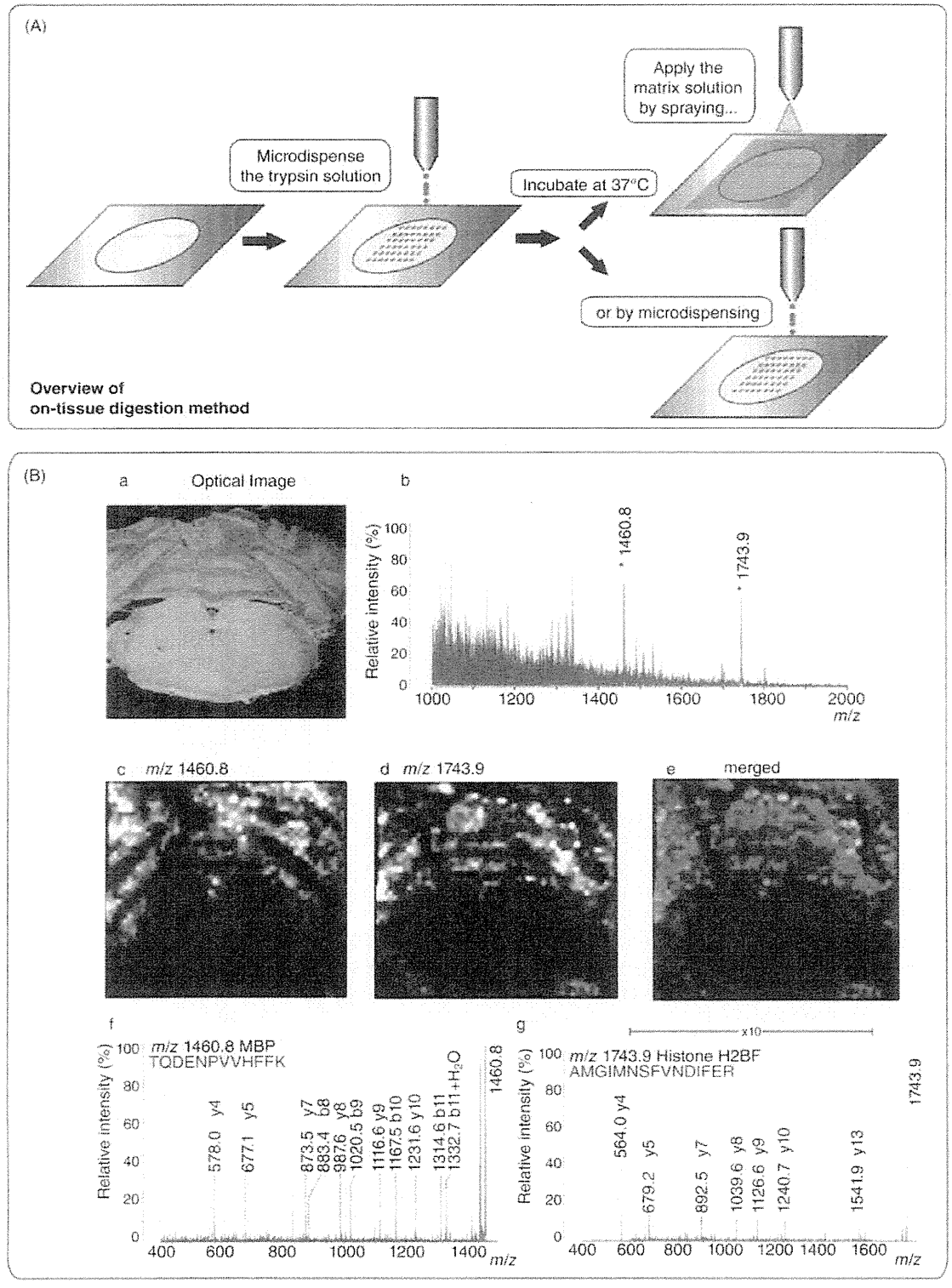

FIGURE 3.8 Tryptic-digested protein imaging and precursor ion mass spectra with positive ion detection mode. A. A scheme showing overview of on-tissue digestion method. B. An example of IMS of tryptic-digested proteins. (a) Optical image of imaging region and (b) accumulated mass spectrum from imaging region. (c, d) Imaging results of *m/z* 1460.8 and 1743.9, which are labeled by asterisks in (b). The merged image (*m/z* 1460.8 and *m/z* 1743.9) is shown in (e). These peaks were identified by direct multistage tandem mass spectrometry (MSn) and were identified as the fragment ions of (f) myelin basic protein (MBP) and (g) histone H2B [18].